Published in final edited form as:

Nature. 2017 December 06; 552(7683): 72–77. doi:10.1038/nature24648.

Programmable self-assembly of three-dimensional nanostructures from 10^4 unique components

Luvena L. Ong[1,2], **Nikita Hanikel**[1], **Omar K. Yaghi**[1], **Casey Grun**[1], **Maximilian T. Strauss**[3,4], **Patrick Bron**[5], **Josephine Lai-Kee-Him**[5], **Florian Schueder**[1,3,4], **Bei Wang**[1,6], **Pengfei Wang**[7], **Jocelyn Y. Kishi**[1,8], **Cameron A. Myhrvold**[1,8], **Allen Zhu**[1], **Ralf Jungmann**[3,4], **Gaetan Bellot**[9], **Yonggang Ke**[7,10], and **Peng Yin**[1,8]

[1]Wyss Institute for Biologically Inspired Engineering, Harvard University, Boston, MA 02115, USA

[2]Harvard-MIT Division of Health Sciences and Technology, Massachusetts Institute of Technology, Cambridge, MA 02139, USA

[3]Max Planck Institute of Biochemistry, 82152 Martinsried Munich, Germany

[4]Department of Physics and Center for Nanoscience, Ludwig Maximilian University, 80539 Munich, Germany

[5]Centre de Biochimie Structurale, CNRS UMR 5048, INSERM U1054, F-34000 Montpellier, France

[6]Department of Polymer Science and Engineering, University of Science and Technology of China, Hefei, Anhui 230026, China

[7]Department of Biomedical Engineering, Emory University and Georgia Institute of Technology, Atlanta, GA 30322, USA

[8]Department of Systems Biology, Harvard Medical School, Boston, MA 02115, USA

[9]Institut de Génomique Fonctionnelle, CNRS UMR 5203, INSERM U1191, F-34000 Montpellier, France

[10]Department of Chemistry, Emory University, Atlanta, GA 30322, USA

Abstract

Nucleic acids (DNA and RNA) are widely used to construct nanoscale structures with ever increasing complexity[1–14] for possible applications in fields as diverse as structural biology,

Correspondence to: Gaetan Bellot; Yonggang Ke; Peng Yin.

Author contributions: L.L.O. conceived the project, designed and performed the experiments, analyzed the data, and wrote the paper. N.H. designed and performed the experiments, analyzed the data, and wrote the paper; O.K.Y., B.W. and P.W. performed the experiments and analyzed the data. M.T.S. and F.S. performed the 3D DNA-PAINT experiments, analyzed the data, and wrote the paper. C.G. and J.Y.K. developed the Nanobricks software and wrote the paper. P.B. and J.L. performed the electron tomography experiments. C.A.M. designed and analyzed the sequencing experiments and wrote the paper. A.Z. performed the experiments. R.J. supervised the DNA-PAINT experiments, interpreted data, and wrote the paper. G.B. designed and supervised the electron tomography study, interpreted data, and wrote the paper. Y.K. and P.Y. conceived, designed, and supervised the study, interpreted the data, and wrote the paper.

Competing financial interests: A patent has been filed based on this work. P.Y. is co-founder of Ultivue Inc. and NuProbe Global.

biophysics, synthetic biology and photonics. The nanostructures are formed through one-pot self-assembly, with early examples typically containing on the order of 10 unique DNA strands. The introduction of DNA origami[4], which uses many staple strands to fold one long scaffold strand into a desired structure, gave access to kilo- to mega-dalton nanostructures containing about 10^2 unique DNA strands[6,7,10,13] . Aiming for even larger DNA origami structures is in principle possible[15,16], but faces the challenge of having to manufacture and route an increasingly long scaffold strand. An alternative and in principle more readily scalable approach uses DNA brick assembly[8,9], which doesn't need a scaffold and instead uses hundreds of short DNA brick strands that self-assemble according to specific inter-brick interactions. First-generation bricks used to create 3D structures are 32-nt long with four 8-nt binding domains that directed 10^2 distinct bricks into well-formed assemblies, but attempts to create larger structures encountered practical challenges and had limited success.[9] Here we show that a new generation of DNA bricks with longer binding domains makes it possible to self-assemble 0.1 – 1 giga-dalton three-dimensional nanostructures from 10^4 unique components, including a 0.5 giga-dalton cuboid containing 30,000 unique bricks and a 1 giga-dalton rotationally symmetric tetramer. We also assemble a cuboid containing 10,000 bricks and 20,000 uniquely addressable 'nano-voxels' that serves as a molecular canvas for three-dimensional sculpting, with introduction of sophisticated user-prescribed 3D cavities yielding structures such as letters, a complex helicoid and a teddy bear. We anticipate that, with further optimization, even larger assemblies might be accessible and prove useful as scaffolds or for positioning functional components.

Without altering the fundamental design principle of the original 32-nt DNA bricks, we empirically optimized domain dimensions to generate the new 52-nt DNA bricks that allow the self-assembly of 0.1 – 1 gigadalton structures from 10^4 bricks (Fig. 1a, b). We investigated structure formation yields by tuning the brick lengths to 52 nt (four 13-nt domains) or 74 nt (two 18-nt and two 19-nt domains), such that the inter-brick binding pattern remains perpendicular. For example, two neighboring 52-nt DNA bricks form a 13-basepair (bp) duplex that corresponds to a 90° inter-brick angle. Comparing 6 helices (H) ×6H×8*x* base pairs (B), where×= {8, 13, 18.5}, we find that cuboids assembled from 52-nt bricks show substantially higher formation yields in both 72-hour thermal annealing (Supplementary Figs. 4, 6, 7, and 8) and isothermal annealing reactions (Supplementary Figs. 5, 11, Supplementary Table 2) than the other two brick structures. Direct comparison of 52-nt brick structures and 32-nt brick structures with similar overall dimensions also revealed that 52-nt brick structures assemble with higher yield and thermal stability (Supplementary Figs. 9 – 12).

Given the importance of annealing conditions, we tested the influence of a number of factors including salinity, temperature ramps, and reaction times on the folding of a 20H×20H×260B structure at a 5 nM strand concentration to obtain an optimal protocol. This 67.6 MDa cuboid had the highest gel yields of ~6% after annealing in 20 mM $MgCl_2$ isothermally at 51.4°C, or when using a 1.5°C narrow annealing ramp (52.5 °C to 51°C) over 5 – 7 days (Supplementary Figs. 16, 17).

Scalability is demonstrated by assembling the cuboids 10H×10H×156B, 14H×14H×208B, 20H×20H×260B, 30H×30H×260B, 36H×36H×312B, 40H×40H×338B, 46H×46H×390B,

which range in size from 10.1 to 536 MDa and were annealed isothermally in one-pot reactions with 20 mM $MgCl_2$ (Fig. 2a, in grey). Using an 8H×8H×104B 4.3 MDa origami structure as benchmark (Fig. 2a, b, in blue; Supplementary Figs. 19 – 22), gel electrophoresis analysis indicates 1 – 20% formation yields that depend on the size of the structure and the strand concentration (Fig. 2a, Extended data fig. 1). Each structure has an optimal formation temperature range that tends to narrow as the complexity of the structure increases (Supplementary Fig. 18), suggesting that increased sequence diversity and larger number of components may limit effective nucleation and growth to a smaller window of reaction conditions. Transmission Electron Microscopy (TEM) revealed complete structures with expected dimensions and morphologies using purified samples (Fig. 2, Supplementary Figs. 23 – 46), along with some defective structures (Supplementary Fig. 36) that may reflect incomplete assembly or post-assembly damage during gel purification or TEM sample preparation.

The 46H×46H×390B cuboid, with a size of 536.4 MDa that is over 100 times that of an M13 scaffolded DNA origami[4], is the largest assembled structure composed of entirely unique components (Fig. 2b, Supplementary Fig. 43). It measures over 100 nm in each dimension, contains over 30,000 unique components (33,511 strands) with ~1.7 million nucleotides, and forms with over 1% gel yield. Due to the symmetry present in DNA brick structures, discrete multimer structures can be created by connecting strands across different symmetric planes[17] (Supplementary Figs. 47 – 58). We applied a side-to-side tetramer design to assemble a 1 gigadalton tessellation structure, which measures 72H×72H×312B and contains four identical 262.8 MDa monomeric units (see Supplementary Figs. 59–61 for design details). This was implemented by utilizing the C4 symmetry[17] present in the plane perpendicular to the DNA helical axis, with strands designed to connect one face of the structure, parallel to the helical axis, to an adjacent face of the same orientation to give a rotationally symmetric tetramer (Fig. 2c–e, Supplementary Figs. 62 – 64). This gigadalton structure also forms through a simple one-pot isothermal annealing reaction with ~1% gel yield, with TEM confirming that its morphology is as designed (Extended data fig. 1h, Supplementary Figs. 62 – 64, Supplementary Figs. 62, 63). A defect seen in the center of some particles seems likely due to the putative strain accumulated at the center of the tetramer.

The high component complexity of these cuboids also enables them to be used as programmable “molecular canvases” for complex shape patterning. As a demonstration, we selected the 30H×30H×260B cuboid, which is assembled from 9,700 unique bricks, measures 152 megadalton, and offers 18,000 voxels at a resolution of 13 bp per voxel (Fig. 1c, d). TEM imaging of this cuboid showed that 90% of the particles exhibited expected morphology with no severe distortions (Supplementary Fig. 83), and 3D DNA-PAINT super-resolution imaging[11,18] further confirmed the expected dimensions for the particles in solution and revealed that all eight corners of most structures are intact (Fig. 2f model, Supplementary Figs. 65, 66).

To facilitate user-friendly design of large 3D brick structures containing the order of 10^4 components, we developed a software tool called *Nanobricks*. First, the user draws, imports, or programs (e.g. via mathematical scripting) a 3D shape by placing “voxels” that represent

DNA strand domains. The software then converts the shape into associated DNA brick strands. Finally, the software outputs sequences by generating new or applying an existing set of sequences to the strands (Fig. 3a). The software contains features to add, remove, or modify on the voxel or strand level for each of three steps (Fig. 3a, Supplementary Figs. 67 – 74), and can output file formats compatible with other commonly used DNA structure design and analysis tools[19] (see Supplementary Section S8.4).

We used Nanobricks to design 13 distinct complex cavity shapes from the 30H×30H×260B canvas (Fig. 3, Extended Data Fig. 2, Supplementary Figs. 75 – 83, and Supplementary Table 3). The shapes were designed using shape importing, mathematical scripting, manual designing or a combination of these methods. Nanobrick's user-friendly 3D visualization and editing interface allowed for easy manipulation of the 18,000 voxels of the molecular canvas (Supplementary Figs. 67 – 74). To determine the minimal feature size, we patterned the surface of a hollow cuboid with varying pore sizes and found that a minimum of 4 helices between separated design features was needed for the structure to form completely (Extended data fig. 2b). Implementing these restrictions, we used the software to convert several open-source 3D designs to voxelized approximations (Figs. 3b, e, f, and Supplementary Fig. 76). Scripting capabilities allowed for design of complex mathematical cavities, including a helicoid, Möbius strip, hyperboloid, and cone, by identifying whether voxels were located within a given mathematical formula (Figs. 3c, g–i and Supplementary Section S9.4). Manual designs include a structure featuring the projections of "G", "E", and "B" along three axes (fig. 3d), one exhibiting the word "LOVE" in one single projection (Figs. 3e), one containing two interconnected loop cavities (Fig. 3j), one with a cavity that threads through itself (Fig. 3k), and other complex shapes (Fig. 3l, m, n).

No "protector strands"[9] were used within the cavities (Supplementary Fig. 75). Surprisingly, these structures showed strong tolerance to the presence of a large number of exposed "sticky" single-stranded ends inside the cavities, and assembled at yield between 1.5 and 5.1% (Extended data fig. 2c). TEM characterization of the different shapes further showed that approximately 75% of the structures were intact and displayed the expected internal cavities (Supplementary Fig. 83).

Complex structural features were also analyzed in detail by using electron tomography (Fig. 4). We first performed 3D reconstruction on a 30H×30H×260B cuboid with sixteen-parallel 2H×2H×260B crossing channels (Fig. 4a, b). The reconstructions and the 3D visualization using mesh surface representation revealed the 3D channels network in the cuboid. The global topology of the reconstructed density is in agreement with the expected architecture of the object and showed typical shape artifacts at the extreme top and bottom of the particles in the direction of the electron beam due to the missing wedge.[20] We then performed electron tomography on four distinct cavity structures: teddy bear, bunny, helicoid, and "GEB" (Fig. 4a–c, e, Supplementary Figs. 86 – 93, and Supplementary Movies). Tilt-series images were collected for each of the three projection views to validate the fine 3D features. Thin features containing only few voxels, such as the teddy bear's snout and limbs (red arrows in Fig. 4e) or the bunny's ears (Supplementary Figs. 91 – 93), were confirmed through reconstructions.

To quantitatively examine the incorporation of each of the 10^4 bricks into the structure, we applied a DNA sequencing-based analysis[21] on the teddy bear structure. The assembled structure was gel purified and heat denatured. The resulting DNA strands were ligated with sequencing primers, amplified, sequenced, and compared with a sample of unreacted strands[21](see Supplementary Sections S11.1 and S11.2). Strands with a sequencing read number below a specific threshold are designated as low abundance. By applying this threshold-based analysis to all strands of the molecular canvas, we can extract information about the abundance of each strand in the formed product and thus the average voxel composition of the formed teddy-bear cavity structure (Fig. 5, Supplementary Figs. 104 – 112). Such analysis revealed that the majority (>98%) of the strands forming the teddy bear structure were present in high abundance according to our sequencing analysis (Supplementary Fig. 105), and only a small number of sparsely distributed voxels exhibited undesired low abundance (red voxels in Fig. 5a and Supplementary Figs. 105 – 106). Projections of the low abundance strands data along the different axes matched the expected projections of the design (Fig. 5b, Supplementary Figs. 111, 112). By normalizing the data, we observed a “hot spot” of low-abundance strands at the back of the teddy bear, which is consistent with some broken particles observed by TEM (Supplementary Fig. 112). This structural defect could potentially be caused by the presence of only a few crossovers at this tenuous spot.

The successful construction of large and complex structures appears the result of the 52-nt bricks being able to mitigate the slow assembly kinetics that inevitably arises with the decreased component concentration encountered when assembling large DNA structures from a massive number of distinct components. While the detailed mechanism of brick structure formation remains to be explored, our results are consistent with the hypothesis that assembly involves delayed nucleation followed by fast growth.[9,28] In our case, we find that domain lengthening from 8-nt to 13-nt results in structures forming more rapidly. We also note that binding heterogeneity has been found to circumvent the emergence of multiple dominant competing nuclei[28], implying that component heterogeneity is further enhanced in our 52-nt brick design because the range of accessible binding energies becomes wider with longer domains due to the larger sequence space.

The 0.5 GDa structure we have constructed contains 33,511 unique components, 1,684,336 nt of sequence, and bridges two orders of magnitude in length in all three dimensions in a space filling fashion: from a feature resolution of $2.8\times2.8\times4.4$ nm^3 to assembled structures with an 100 nm length in each of the three dimensions. Although the present work focuses on constructing compact, spacing filling structures with 10^4 unique components packed in 1 attolitre (i.e. $100\times100\times100$ $nm^3 = 10^{-21}m^3$) space, it should also be feasible to use variations of the bricks to construct wire-frame or porous structures[10,11,13,14] with similar component complexity. Considering that the 10-fold leap in component complexity afforded by DNA origami opened the door for using DNA nanostructures in fields as diverse as single molecule biophysics,[22] structural biology,[23] synthetic biology,[24] nanofabrication,[25,26] and photonics[27], we anticipate that the 100-fold increase in complexity afforded by our DNA brick method will also enable new uses for DNA nanostructures (e.g. as scaffolds for patterning complex inorganic nanostructures[25] or for 3D positioning of diverse functional moieties[26,27]). In fact, even large DNA brick assemblies might be possible, considering that

the high cost of purchasing a large number of synthetic DNA strands has restricted our testing to ~30,000 distinct bricks and that low-cost methods for synthesizing DNA strands (e.g. chip-synthesized DNA followed by parallel enzymatic amplification[29]) are available. Further scaling-up of assembly size could also be achieved by hierarchical methods via sticky end association or shape complementarity.[12,30]

Methods

Condensed descriptions of methods are described below. See the Methods section in the Supplementary Information for specific details.

Design and formation of structures

Structures were designed using our Nanobricks software. Depicted 2D strand diagrams were generated from associating caDNAno files.[19] Structures were annealed in 0.5×TE buffer (5 mM Tris, 1 mM EDTA, pH 8) containing 20 mM $MgCl_2$ using either an isothermal hold[31] or a narrow annealing ramp. See Supplementary Methods and Supplementary Table 1 for the detailed annealing conditions and optimal temperatures. See supplementary information for sequences used for each structure.

Agarose gel electrophoresis

Samples were analyzed using 0.3–2% agarose gel electrophoresis and stained using SYBR Safe loading dye. Gels were visualized using the Typhoon FLA 9000 gel imager and quantified using ImageJ[32] or TotalLabQuant v12.2 (Cleaver Scientific, ltd).

Transmission electron microscopy imaging

Samples were deposited on glow-discharged formvar/carbon coated grids from Electron Microscopy Sciences. Samples were stained for 60 seconds with 2% uranyl formate solution containing 25 mM NaOH and imaged using a JEOL JEM-1400 TEM operated at 80 kV.

Electron tomography and image processing

Samples were deposited on glow-discharged, carbon-coated 300 mesh copper grids and stained using 1% uranyl acetate solution. The grids were then transferred into a JEOL 2200FS FEG transmission microscope using the JEOL high tilt holder. Series of tilted images were collected at a magnification of 50,000 folds by using a 4k × 4k slow-scan CCD camera (Gatan, inc.) with defocus values of −3 μm and −5 μm. The acquisition was performed semi-automatically using the Serial EM software package. Samples were tilted between −60° and 60° with 2° increment steps. For a detailed description of the alignment and reconstruction procedure see the Supporting Information.

3D DNA-PAINT super-resolution setup

Fluorescence imaging was performed using an inverted Nikon Eclipse Ti-E microscope (Nikon Instruments, Melville, NY) with the Perfect Focus System, applying an objective-type TIRF configuration with an oil-immersion objective (CFI Apo TIRF 100×, NA 1.49, Oil). 3D images were acquired using a cylindrical lens (FL = 1m) in the detection path.

Super-resolution DNA-PAINT images were reconstructed using spot-finding and 2D-Gaussian fitting algorithms programmed in LabVIEW.[18] A previously published calibration function[33] was used for 3D calibration. Drift correction was performed on the DNA structures, as previously described.[34]

Z-calibration was additionally corrected for refractive-index-mismatch by measuring a reference structure with given height, resulting in a correction factor of 1.3.[11] ViSP[35] was used to visualize single-particle localizations in three dimensions. After exporting from ViSP, images and corresponding color bars were contrast-adjusted using Fiji.[36] See the Supplementary Methods for additional details on sample preparation and image analysis.

Sequencing sample preparation and analysis

Sequencing analysis was prepared following a modified version of the barcode extension for analysis and reconstruction of structures (BEARS) protocol.[21] Samples were ligated to an adaptor sequence on the 5' end using T4 RNA ligase 1 (New England Biolabs) and purified using polyacrylamide gel electrophoresis and electroelution. Subsequently, the 3' end of the strands was ligated to a previously tested adaptor sequence[21] containing an integrated barcode. Then samples were amplified using Q5 polymerase.

Multiple samples with different barcodes were pooled and sequenced with an Illumina MiSeq machine according to the manufacturer's instructions by using the MiSeq V2 paired end 50 kit (Illumina Inc., San Diego, CA). A modified library denaturation and loading protocol for lower concentration libraries was used.[37]

Data availability

The authors declare that the main data supporting the findings of this study are available within the paper and its Supplementary Information files. Sequences used to form the large structures are provided as well. Structure designs and software are posted at https://yin.hms.harvard.edu/bricks/try/#. All other data supporting the findings of this study are available from the corresponding authors on request.

Extended Data

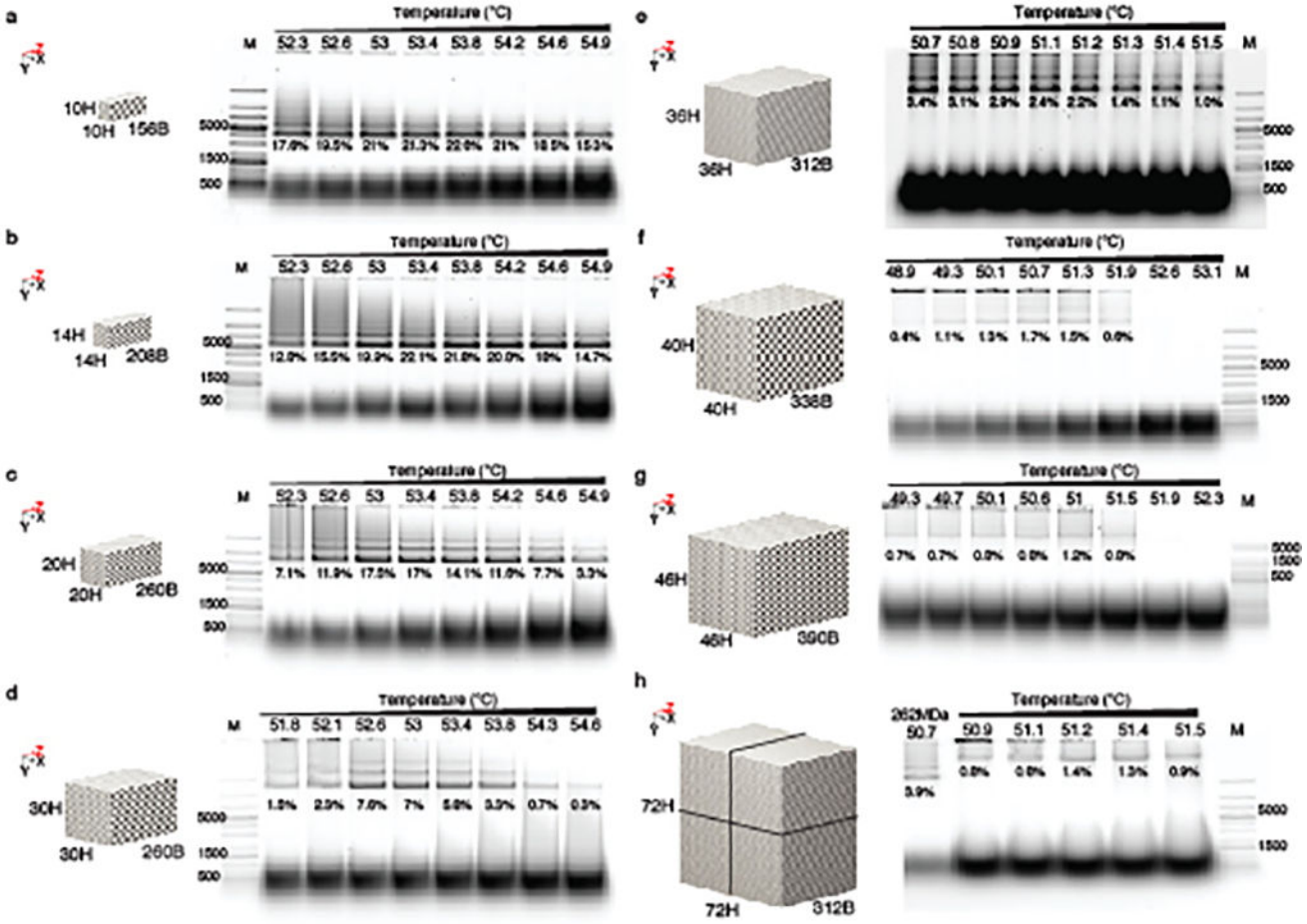

Extended Data Figure 1. Gel electrophoresis analysis of DNA brick cuboids

Structures were assembled isothermally for 5 – 7 days at the temperatures indicated above the lane. The label below a band of interest indicates the gel yield.

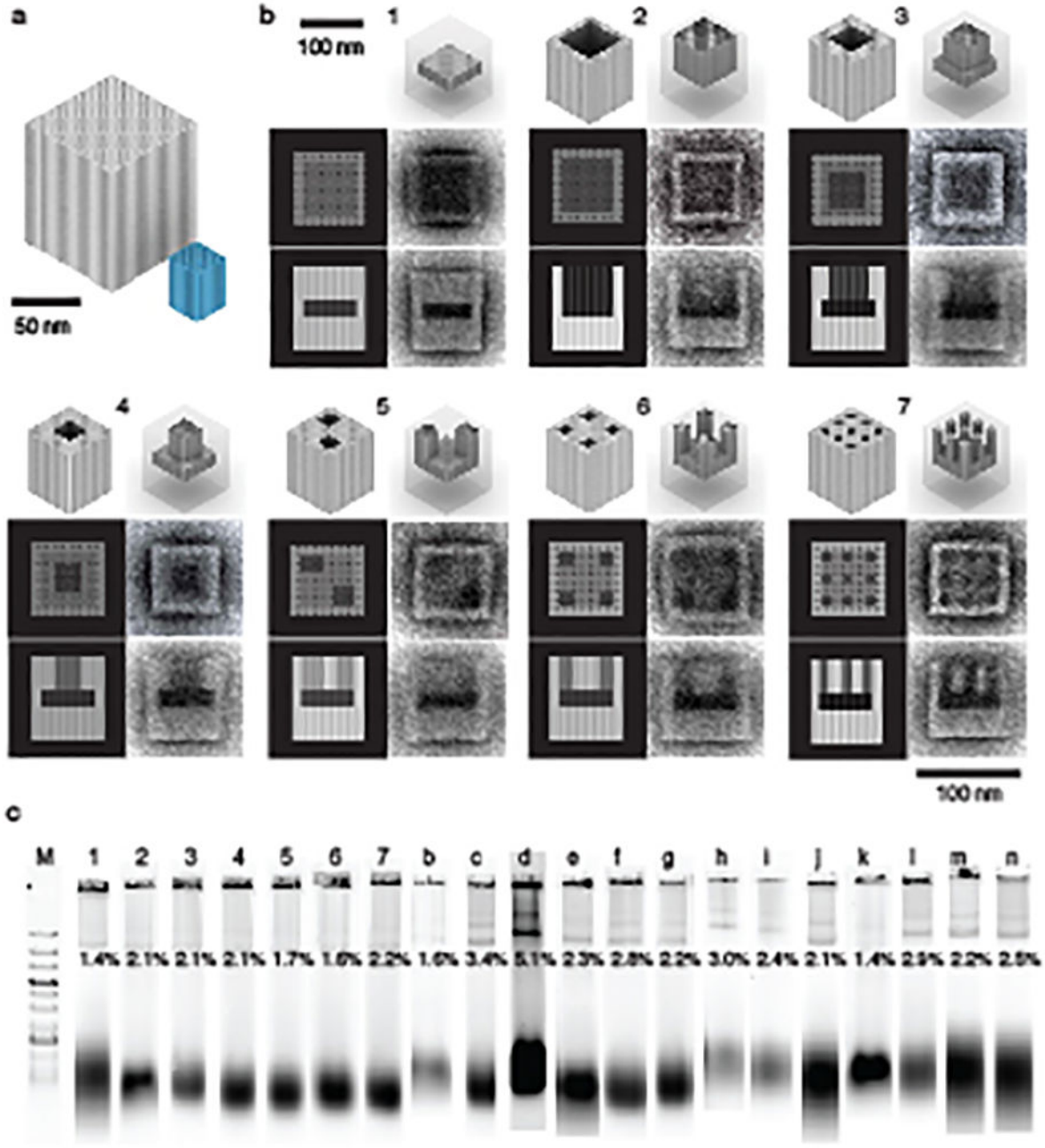

Extended Data Figure 2. Characterization of 30H×30H×260B cavity shapes

a, Schematic depicting the 30H×30H×260B molecular canvas in gray compared with a DNA origami-sized structure in blue. **b,** For each structure, the top panels show the 3D models of the designed structure. The bottom left panels shows expected TEM projections. The bottom right panels shows TEM averages from at least six particles. **c,** The structures were folded with 5 nM/strand by annealing isothermally or using a narrow ramp from 52.5 to 51°C. Products were analyzed on a 0.5% agarose gel in the presence of 10 mM $MgCl_2$. The percentage number listed below a target band indicates the gel yield. Lane labels correspond to those in Fig. 3 and in **(b)**.

Supplementary Material

Refer to Web version on PubMed Central for supplementary material.

Acknowledgments

The authors thank N. Ponnuswamy, R. Sørensen, J. Hahn, J. Lara, L. Chou, N. Garreau, S. Saka, H. Sasaki, J.B. Woehrstein, and C.B. Marks for experimental help. The authors also thank B. Wei, W. Sun, and W.M. Shih for insightful discussions, M. Beatty and J. Cheng for help in developing the Nanobricks platform, and C. Chen for assistance with draft preparation. The work was funded by Office of Naval Research grants N000141010827, N000141310593, N000141410610, and N000141612182, and N000141612410, an Army Research Office grant W911NF1210238, National Science Foundation grants CCF-1054898, CCF-1162459, CCF-1317291, CMMI-1333215, CMMI-1334109, CMMI-1344915, an Air Force Office of Scientific Research grant AFA9550-15-1-0514, National Institute of Health grants 1DP2OD007292 and 1R01EB018659, 167814, (P.Y.); An Emory Biomedical Engineering Department Startup Fund, an Emory Winship Cancer Institute Billi and Bernie Marcus Research Award, an Winship Cancer Institute grant #IRG-14-188-0 from the American Cancer Society, an National Science Foundation CAREER Award DMR–1654485 (Y.K.); French National Research Agency grants ANR-16-CE09-0004-01, ANR-15-CE09-0003-02 (G.B.); an French National Research Agency grant ANR-10-INBS-05 (P.B.). L.L.O. was funded by an NSF graduate research fellowship. N.H. was funded by the German National Academic Foundation and German Academic Exchange Service. M.T.S. acknowledges support from the International Max Planck Research School for Molecular and Cellular Life Sciences (IMPRS-LS).

References

1. Chen J, Seeman NC. The synthesis from DNA of a molecule with the connectivity of a cube. Nature. 1991; 350:631–633. [PubMed: 2017259]
2. Winfree E, Liu F, Wenzler LA, Seeman NC. Design and self-assembly of two-dimensional DNA crystals. Nature. 1998; 394:539–544. [PubMed: 9707114]
3. Shih WM, Quispe JD, Joyce GF. A 1.7-kilobase single-stranded DNA that folds into a nanoscale octahedron. Nature. 2004; 427:618–621. [PubMed: 14961116]
4. Rothemund PWK. Folding DNA to create nanoscale shapes and patterns. Nature. 2006; 440:297–302. [PubMed: 16541064]
5. Zheng JP, et al. From molecular to macroscopic via the rational design of a self-assembled 3D DNA crystal. Nature. 2009; 461:74–77. [PubMed: 19727196]
6. Douglas SM, et al. Self-assembly of DNA into nanoscale three-dimensional shapes. Nature. 2009; 459:414–418. [PubMed: 19458720]
7. Han D, et al. DNA origami with complex curvatures in three-dimensional space. Science. 2011; 332:342–346. [PubMed: 21493857]
8. Wei B, Dai M, Yin P. Complex shapes self-assembled from single-stranded DNA tiles. Nature. 2012; 485:623–626. [PubMed: 22660323]
9. Ke Y, Ong LL, Shih WM, Yin P. Three-dimensional structures self-assembled from DNA bricks. Science. 2012; 338:1177–1183. [PubMed: 23197527]
10. Han D, et al. DNA gridiron nanostructures based on four-arm junctions. Science. 2013; 339:1412–1415. [PubMed: 23520107]
11. Iinuma R, et al. Polyhedra self-assembled from DNA tripods and characterized with 3D DNA-PAINT. Science. 2014; 344:65–69. [PubMed: 24625926]
12. Gerling T, Wagenbauer KF, Neuner AM, Dietz H. Dynamic DNA devices and assemblies formed by shape-complementary, non-base pairing 3D components. Science. 2015; 347:1446–1452. [PubMed: 25814577]
13. Benson E, et al. DNA rendering of polyhedral meshes at the nanoscale. Nature. 2015; 523:441–444. [PubMed: 26201596]
14. Veneziano R, et al. Designer nanoscale DNA assemblies programmed from the top down. Science. 2016; 352:1534. [PubMed: 27229143]
15. Marchi AN, Saaem I, Vogen BN, Brown S, Labean TH. Towards larger DNA origami. Nano Letters. 2014; 14:5740–5747. [PubMed: 25179827]

16. Nickels PC, et al. DNA origami structures directly assembled from intact bacteriophages. Small. 2014; 10:1765–1769. [PubMed: 24532395]
17. Liu Y, Ke Y, Yan H. Self-assembly of symmetric finite-size DNA nanoarrays. J. Am. Chem. Soc. 2005; 127:17140–17141. [PubMed: 16332034]
18. Jungmann R, et al. Multiplexed 3D cellular super-resolution imaging with DNA-PAINT and Exchange-PAINT. Nature Methods. 2014; 11:313–318. [PubMed: 24487583]
19. Douglas, Shawn M., et al. Rapid prototyping of 3D DNA-origami shapes with caDNAno. Nucleic Acids Research. 2009; 37:5001–5006. [PubMed: 19531737]
20. Weyland M, Midgley PA. 3D electron microscopy in the physical sciences: the development of Z-contrast and EFTEM tomography. Ultramicroscopy. 2003; 96:413–431. [PubMed: 12871805]
21. Myhrvold C, et al. Barcode extension for analysis and reconstruction of structures (BEARS). Nature Communications. 2017; 8:14698.
22. Nickels PC, et al. Molecular force spectroscopy with a DNA origami– based nanoscopic force clamp. Science. 2016; 354:305–307. [PubMed: 27846560]
23. Douglas SM, Chou JJ, Shih WM. DNA-nanotube-induced alignment of membrane proteins for NMR structure determination. Proc. Natl Acad. Sci. USA. 2007; 104:6644–6648. [PubMed: 17404217]
24. Fu J, et al. Multi-enzyme complexes on DNA scaffolds capable of substrate channeling with an artificial swinging arm. Nature Nanotechnology. 2014; 9:531–536.
25. Sun W, et al. Casting inorganic structures with DNA molds. Science. 2014; 346
26. Knudsen JB, et al. Routing of individual polymers in designed patterns. Nature Nanotechnology. 2015; 10:892–898.
27. Acuna GP, et al. Fluorescence enhancement at docking sites of DNA-directed self-assembled nanoantennas. Science. 2012; 338:506–510. [PubMed: 23112329]
28. Jacobs WM, Reinhardt A, Frenkel D. Rational design of self-assembled pathways for complex multicomponent structures. Proc. Natl. Acad. Sci. USA. 2015; 112 63136318.
29. Schmidt TL, et al. Scalable amplification of strand subsets from chip-synthesized oligonucleotide libraries. Nature Communications. 2015; 6:8634.
30. Rajendran A, Endo M, Katsuda Y, Hidaka K, Sugiyama H. Programmed Two-Dimensional Self-Assembly of Multiple DNA Origami Jigsaw Pieces. ACS Nano. 2011; 5:665–671. [PubMed: 21188996]
31. Sobczak, Jean-Philippe J., Martin, Thomas G., Gerling, Thomas, Dietz, Hendrik. Rapid folding of DNA into nanoscale shapes at constant temperature. Science. 2012; 338:1458–1461. [PubMed: 23239734]
32. Schneider CA, Rasband WS, Eliceiri KW. NIH image to ImageJ: 25 years of image analysis. Nature Methods. 2012; 9:671–675. [PubMed: 22930834]
33. Huang B, Wang W, Bates M, Zhuang X. Three-dimensional super-resolution imaging by stochastic optical reconstruction microscopy. Science. 2008; 319:810–813. [PubMed: 18174397]
34. Lin C, et al. Sub-micrometer geometrically encoded fluorescent barcodes self-assembled from DNA. Nature Chemistry. 2012; 4:832–839.
35. El Beheiry M, Dahan M. ViSP: representing single-particle localizations in three dimensions. Nature Methods. 2013; 10:689–690. [PubMed: 23900246]
36. Schindelin J, et al. Fiji: an open-source platform for biological-image analysis. Nature Methods. 2012; 9:676–682. [PubMed: 22743772]
37. Quail MA, et al. A large genome center's improvements to the Illumina sequencing system. Nature Methods. 2008; 5:1005–1010. [PubMed: 19034268]

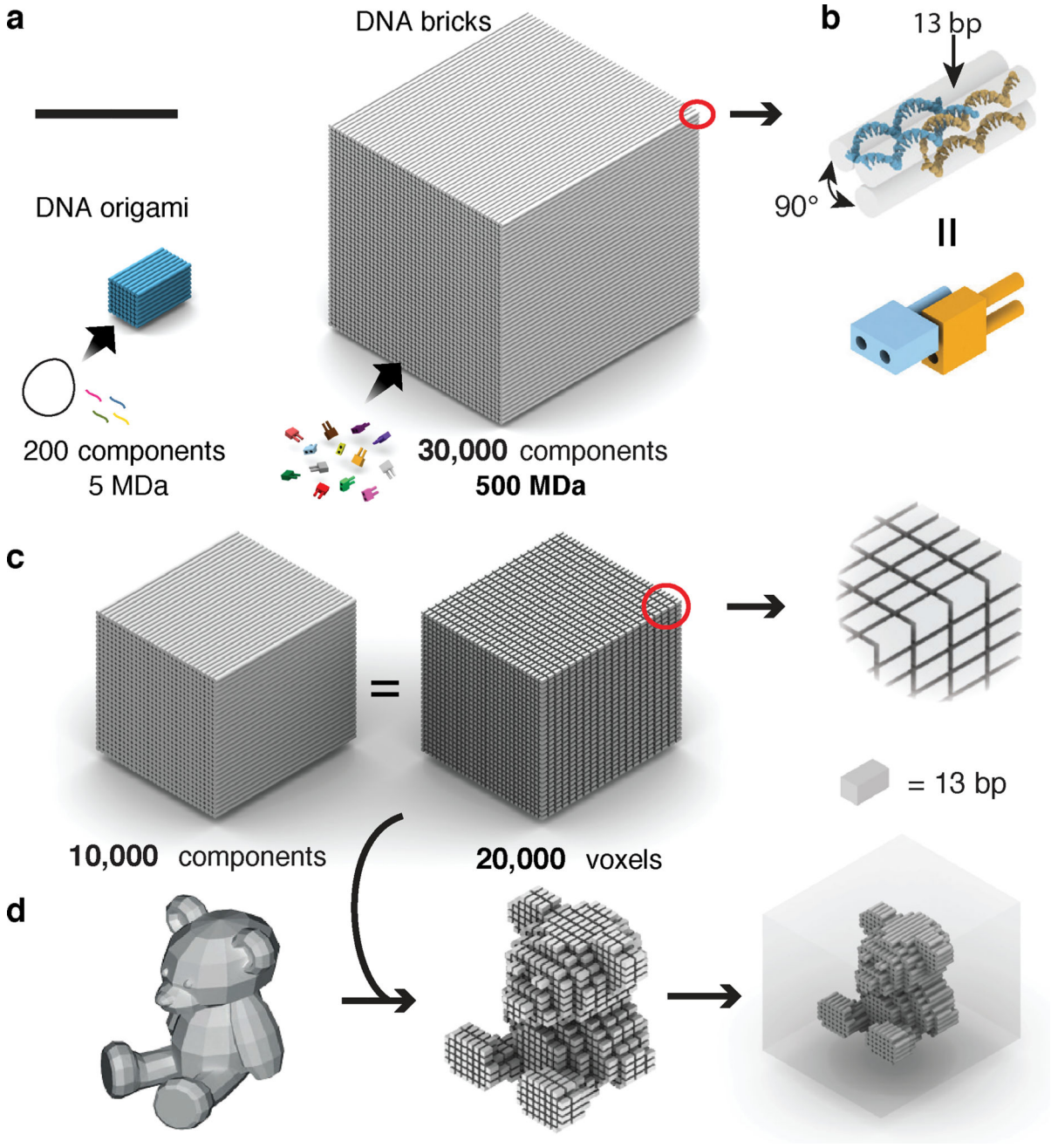

Figure 1. Three dimensional nanostructures self-assembled from DNA bricks

a, Comparison of 3D DNA origami (~200 components, ~5 megadalton),[4] and DNA brick nanostructures assembled here (~30,000 unique components, ~500 megadalton). **b,** Detailed helical (top) and brick (bottom) models of incorporated 52-nt DNA brick strands. **c,** A ~150 MDa DNA brick cuboid (left) as a molecular canvas (middle) composed of ~20,000 13-bp voxels (right). Scale bar in **a** and **c** measures 100 nm. **d,** A 3D teddy bear rendering (left) can be approximated using the ~20,000 voxel canvas (middle) to form the cavity of a cuboid structure (right).

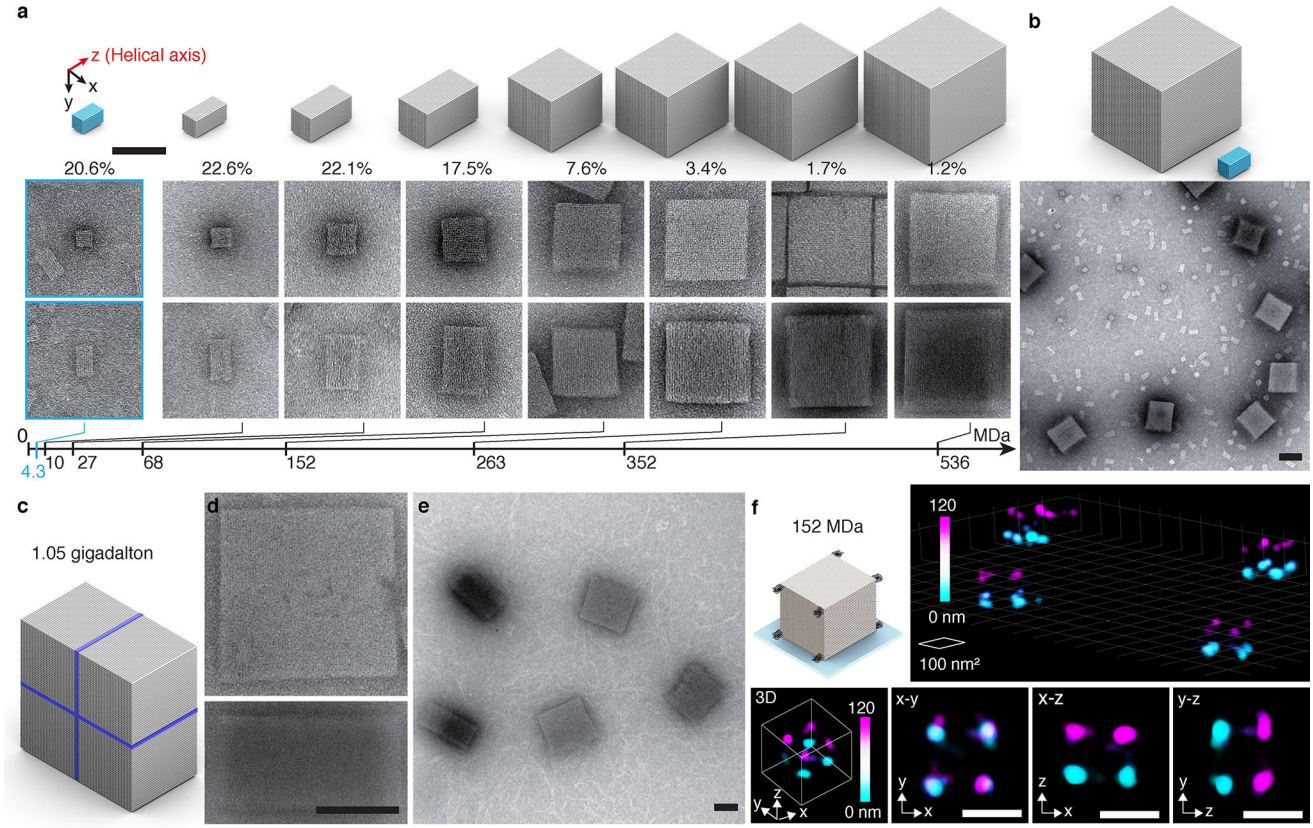

Figure 2. Self-assembly of brick cuboids

Cylindrical models of DNA brick cuboids (gray) and an M13-scaffolded DNA origami cuboid (blue). **a,** Comparison of gel yields (top numbers), TEM images of helical end view (middle), and lateral projection (bottom) of DNA cuboids. **b,** Model (top) and TEM image (bottom) of 536 MDa brick cuboids and 4.3 MDa origami cuboids. 1.05 gigadalton cuboid model **(c)**, selected TEM helical (top) and lateral (bottom) images **(d)**, and wide-field TEM images **(e)**. **f,** 3D DNA-PAINT super-resolution images of the 152 MDa canvas structure: a wide-field view (top) and different projections of a single representative cuboid (bottom). Color bars indicate height along the *z*-axis. All scale bars measure 100 nm.

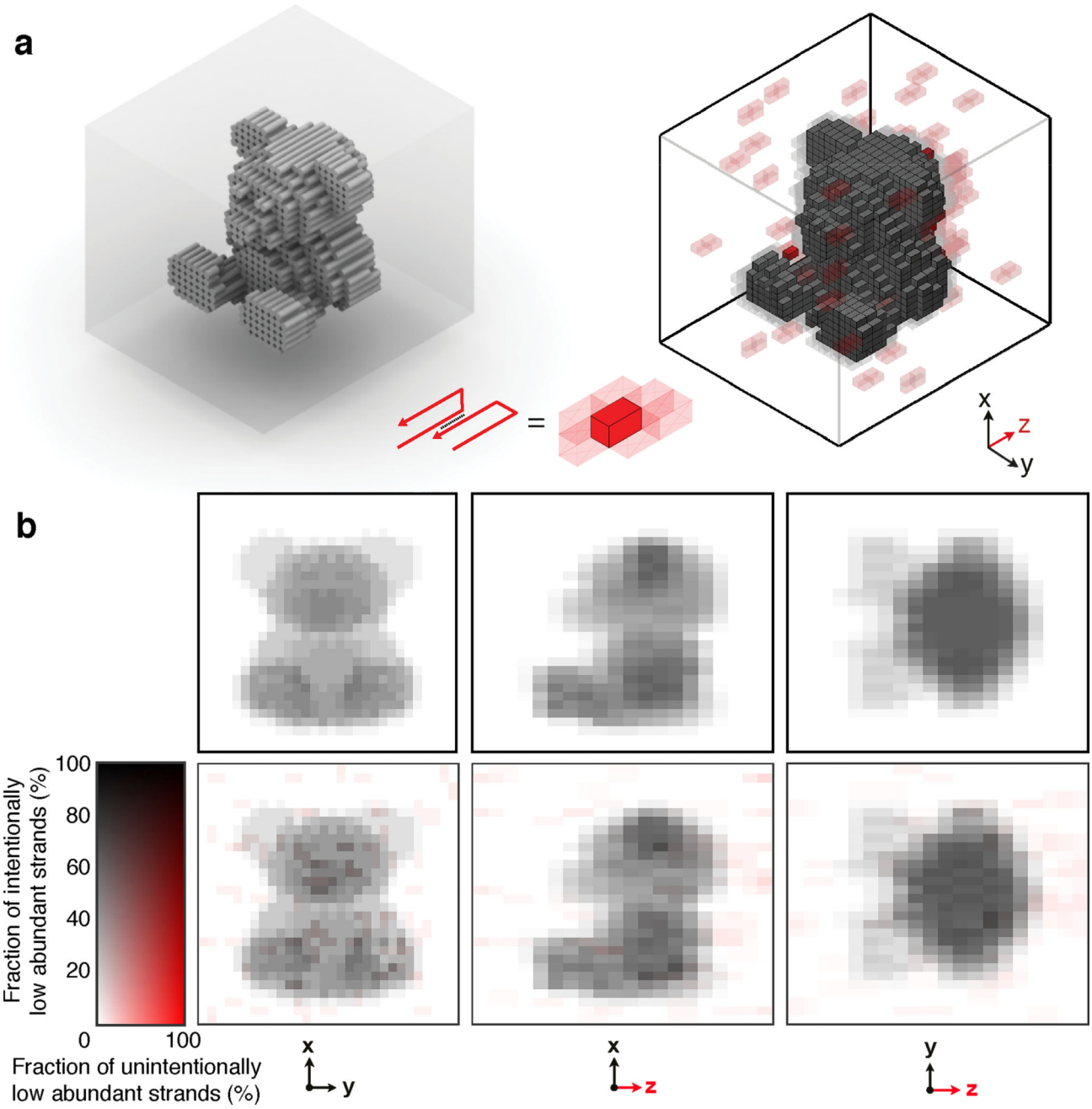

Figure 3. Cavity shapes formed from a 30H×30H×260B molecular canvas

a, Design software for complex DNA brick structures. Desired shapes can be designed by editing voxels through a 3D interface (top), translated automatically to strands (middle), and assigned sequences (bottom). **(b, c)** Cavity shapes can be generated by selecting or excluding (right) voxels to approximate 3D rendering files **(b)** or to satisfy mathematical equations **(c)**. **(d -n)** Diverse cavity shapes. For each design, the top diagram depicts a 3D model of the designed shape. Expected projections (top or left) and averaged TEM images (bottom or right) are also shown. Individual particles used in averaged images are depicted in Supplementary Table 3 and Supplementary Figs. 77 – 82. Scale bars measure 100 nm.

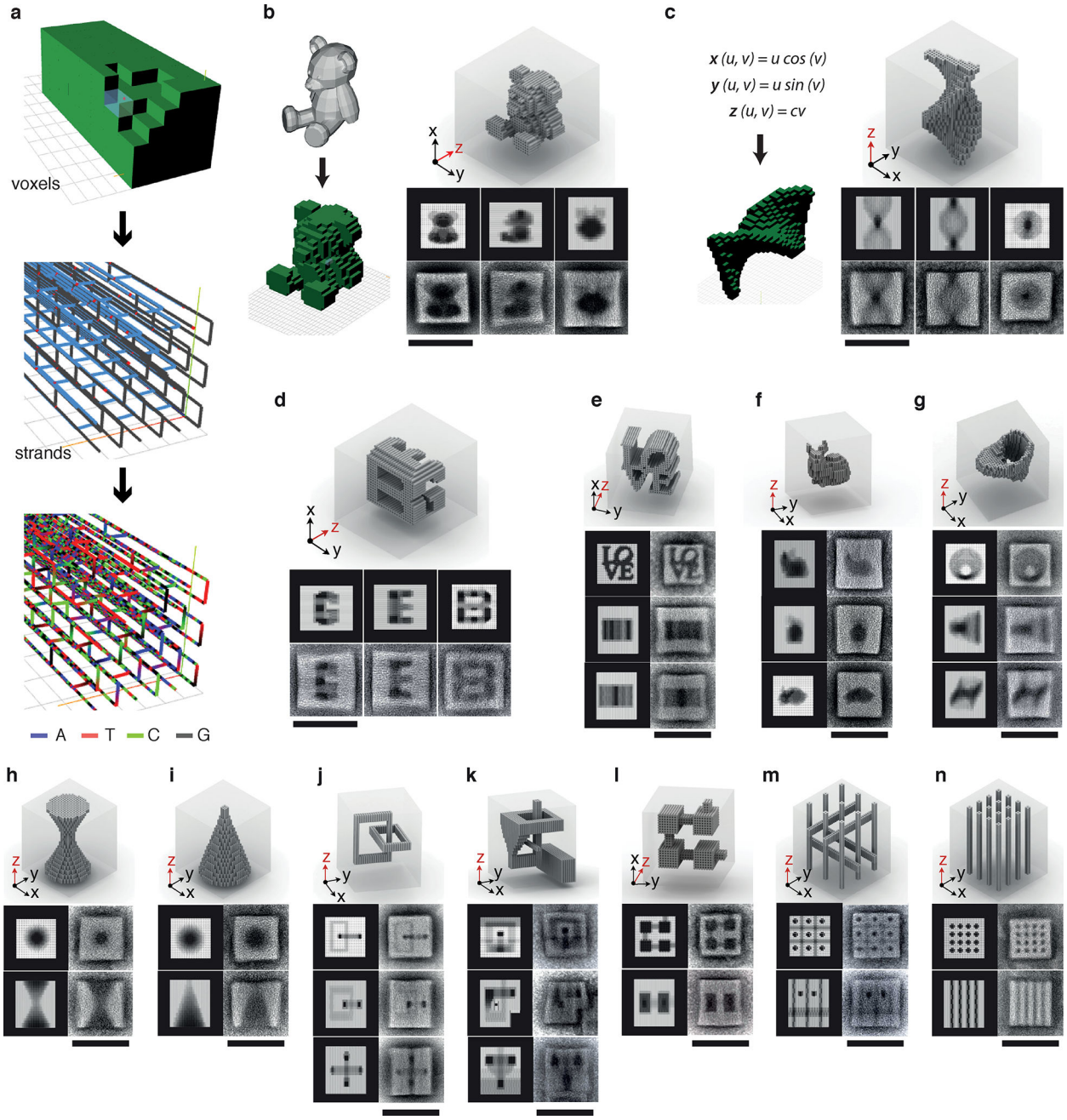

Figure 4. Electron tomography analysis and computational 3D reconstruction of DNA brick structures

a, 3D model of a cuboid containing parallel channels, with extracted slices from the tomogram (right and bottom). **b,** 3D model of the cuboid in a showing the positions of two orthogonal slices (left), and the corresponding 3D mesh-rendered view of their tomographic reconstructions (right). **(c -e),** 3D model (left), expected shape projections (middle), and slices extracted from tomograms (right) for the teddy bear **(c)**, helicoid **(d)**, and "GEB" **(e)** structures. Red arrows point to thin but visible features. Numbers in images correspond to

slice position extracted from each tomogram (see Supplementary Figs. 84 – 93 and Supplementary Movies for more details). All scale bars measure 50 nm.

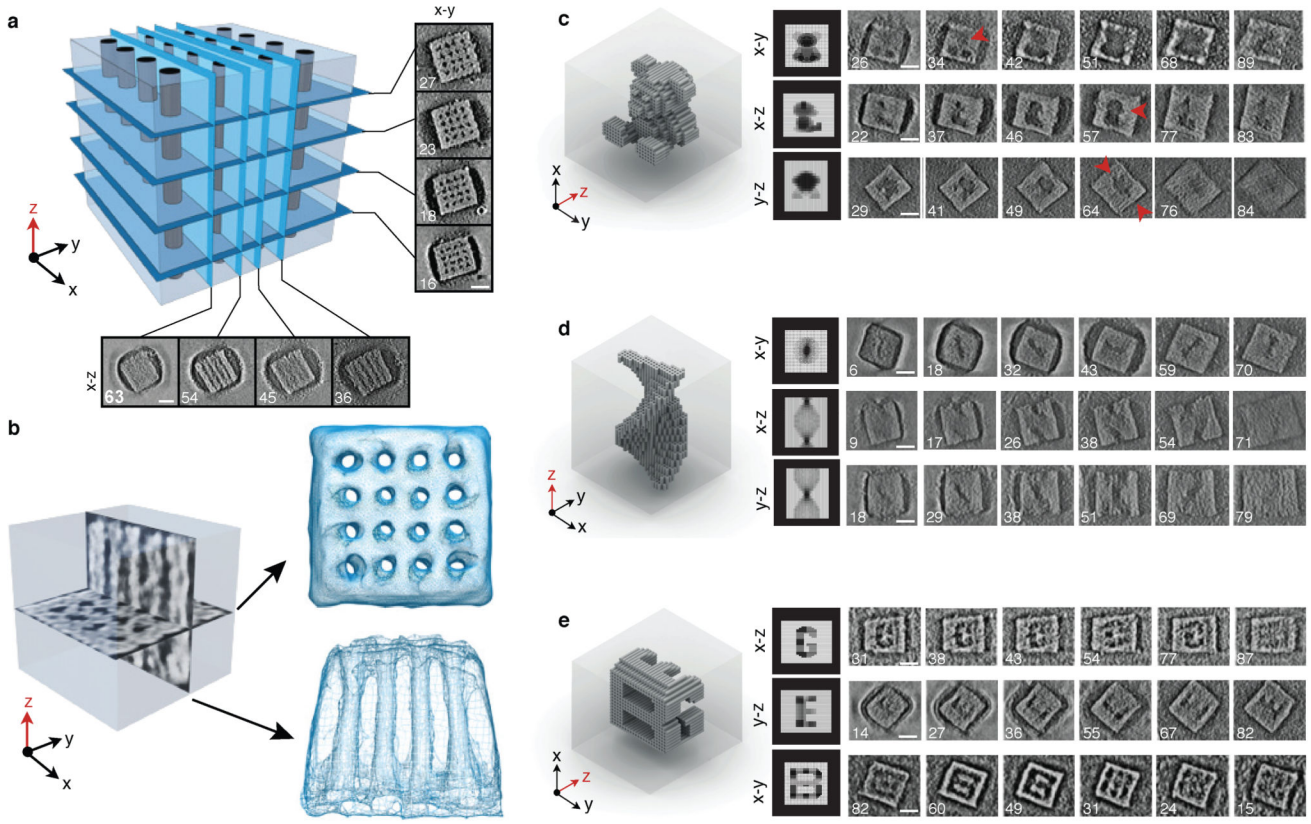

Figure 5. DNA sequencing analysis of the teddy bear cavity structure

a, 3D model (left) and 3D representation of sequencing results (right) of the teddy bear design. Gray and red colors correspond to intended (in cavity) and unintended (in structure) low abundance species, respectively. Opacity of voxels corresponds to the number of strands for which a criterion applies: completely opaque – two, partially transparent – one. Voxels formed by two well incorporated strands are not depicted. **b**, Schematic 2D representations (top) and respective 2D plots of the fractions of low abundance strands along a given axis (bottom).